

Abstract

The Southern Ocean's eddy response to changing climate remains unclear, with observations suggesting non-monotonic changes in eddy kinetic energy (EKE) across scales. Here simulations reappear that smaller-mesoscale EKE is suppressed while larger-mesoscale EKE increases with strengthened winds. This change was linked to scale-wise changes in the kinetic energy cycle, where a sensitive balance between the dominant mesoscale energy sinks - inverse KE cascade, and source - baroclinic energization. Such balance induced a strong (weak) mesoscale suppression in the flat (ridge) channel. Mechanistically, this mesoscale suppression is attributed to stronger zonal jets weakening smaller mesoscale eddies and promoting larger-scale waves. These EKE multiscale changes lead to multi-scale changes in meridional and vertical eddy transport, which can be parameterized using a scale-dependent diffusivity linked to the EKE spectrum. This multiscale eddy response may have significant implications for understanding and modeling the Southern Ocean eddy activity and transport under a changing climate.

Plain Language Summary

The response of eddies in the Southern Ocean to climate change is not well understood. In this study, we used a channel model that simulates the effects of wind on eddies. We found that smaller eddies have less kinetic energy (KE) when the winds are stronger. On the other hand, larger-scale eddies have more KE with stronger winds. Similar phenomena are also observed in the observations. By analyzing the eddy's KE budget, the interaction between different scales of eddies and the interaction between the eddies and mean flow are strengthened when the winds get stronger. This leads to a reduction of eddy KE at smaller mesoscale scales and an increase at larger scales. From the observational view, stronger winds weaken smaller eddies and promote larger waves. This change in eddy KE also affects how eddies meridionally transport materials and how eddy diffusivity varies at different scales. Smaller eddies transport materials less when their KE is weakened, while larger eddies become stronger in transporting materials. These findings determine how eddy diffusivity responds to the changed eddy KE at different scales. The multi-scale response of eddies to wind has important implications for understanding the behavior of Southern Ocean eddies in a changing climate.

1 Introduction

Oceanic eddies play a key role in regulating the Southern Ocean stratification and circulation. These eddies mediate the meridional and vertical exchanges of heat, freshwater, carbon dioxide, nutrients, and other tracers (Ellwood et al., 2020; Frenger et al., 2018; Gnanadesikan et al., 2015; Griffies et al., 2015; Rintoul, 2018; Thompson & Sallée, 2012), while the strong Antarctic Circumpolar Current (ACC) tends to inhibit meridional transport (Siedler et al., 2013). Consequently, the variability of the Southern Ocean eddies has important implications for global ocean circulation and biogeochemical cycles in a changing climate.

The response of eddies to climate change remains an open question and holds particular significance in the Southern Ocean (Rintoul, 2018). Broadly, this inquiry is divided into the response of eddies to two distinct forcings, namely the intensified westerly winds (Swart & Fyfe, 2012; Waugh et al., 2020), and the changing buoyancy forcing in the Southern Ocean (Barkan et al., 2015; Durack et al., 2012; Haumann et al., 2016). Focusing on the strengthened winds, both satellite observations and eddy-resolving models indicated a positive trend in Southern Ocean eddy kinetic energy (EKE) under the historical strengthening of the westerly winds (Morrow et al., 2010; A. M. Hogg et al., 2015; Patara et al., 2016). A similar trend is evident even in global warming simulations (Beech et al., 2022).

65 The EKE, loosely referred to as eddies, in the ocean is composed of variability over
66 a wide range of scales, which may be referred to as the mesoscales ($O(\sim 100\text{--}1000\text{km})$),
67 submesoscales ($O(\sim 1\text{--}50\text{km})$), finescales ($O(\sim 100\text{m})$), or described as a series of
68 coherent features, such as Rossby waves, coherent eddies, jets. The mesoscale variabil-
69 ity composes the dominant fraction of the EKE in the ocean (Wunsch, 2020), and is as-
70 sociated with the main eddy-driven transport. The observational properties of these mesoscales
71 are usually studied through the satellite-based sea surface height (SSH) (Stammer et al.,
72 2006). Some of these studies focused on identifying and quantifying the properties of mesoscale
73 coherent features in SSH anomaly maps (Chelton et al., 2011), while others quantified
74 the variability over the satellite observable range of spatial-temporal scales ($\sim 100\text{km}$
75 and larger) (Storer et al., 2022; Buzzicotti et al., 2023). To focus on the change in mesoscale
76 EKE under strengthened Southern Ocean winds, Martínez-Moreno et al. (2021) refined
77 the definition of mesoscales as scales smaller than 3° and found that this mesoscale EKE
78 increased in response to the winds over the past few decades. Alternatively, Busecke and
79 Abernathey (2019) quantified the changes in bulk lateral mixing mainly due to mesoscale
80 eddies and showed that the interannual variability of mixing was linked to climate in-
81 dices.

82 While these past studies have shown that EKE and specifically mesoscale EKE have
83 responded to strengthened Southern Ocean winds, the multi-scale response to changing
84 winds remains unknown. The distribution of EKE across spatial-temporal scales is set
85 by many competing mechanisms. The generation of the eddies through baroclinic and
86 barotropic instabilities operate at characteristic scales that respond to large-scale strat-
87 ification and flow properties (Smith & Marshall, 2009). This variability is then trans-
88 ferred to other scales through non-linear cascades, which may transfer energy to smaller
89 and larger scales (Klein et al., 2019; Balwada et al., 2022; Garabato et al., 2022). The
90 details of these cascades can also be tied to the large-scale flows and forcing, e.g. Liu et
91 al. (2022) showed that the energy in the coherent mesoscale eddy may be transferred to
92 larger scales (Rossby waves) in the presence of stronger zonal flows. Finally, the diss-
93 ipation mechanisms are also wide and varied, and often linked to boundary processes. In
94 fact, even winds act both as a forcing and a dissipation mechanism, on one hand forc-
95 ing the large-scale state that leads to instability and then the non-linear cascades, and
96 on the other hand killing eddies by applying a drag on the surface flows (Rai et al., 2021;
97 Torres et al., 2022). Thus, the impact of the changing wind forcing in changing the oceanic
98 EKE, particularly its scale-wise spatial-temporal properties, is non-linear and can be quite
99 complex.

100 Understanding the multi-scale response of EKE is important for getting a deeper
101 insight into the energetics that shape the ocean circulation, and consequently a better
102 handle on processes setting the ocean storage and transport. While it is understood that
103 the largest eddies do the bulk of the lateral transport in the ocean, processes like the ver-
104 tical transport of nutrients and ocean ventilation are controlled by flows over a much wider
105 range of scales (Balwada et al., 2018; Uchida et al., 2019). Furthermore, biogeochem-
106 ical processes interact non-linearly with physical transport over a range of time and space
107 scales (Freilich et al., 2022). Additionally, parameterizations of unresolved sub-grid pro-
108 cesses in ocean models are developed by making certain assumptions about energetics
109 (Jansen & Held, 2014; Bachman, 2019), and a better understanding of multi-scale ocean
110 energetics can help inform the improvement and tuning of parameterizations in future
111 ocean models.

112 To investigate this multi-scale aspect, we performed a scale-wise analysis of changes
113 in the geostrophic EKE in different parts of the ACC (Figure S5). This analysis suggests
114 that the changes in the EKE spectrum at different scales are non-monotonic. For exam-
115 ple, observations in the Atlantic sector of the ACC (Figure 1a) indicate an enhancement
116 of larger-scale EKE ($> 180\text{km}$), accompanied by a suppression of smaller mesoscale EKE
117 ($90\text{--}180\text{km}$). The goal of our study here is to probe the dynamics and corresponding

118 impact on the transport of such changes. In general, we employ an idealized mesoscale
 119 eddy-resolving channel model to investigate the multi-scale response of the EKE in the
 120 ACC to strengthened wind forcing. Furthermore, we investigate how these changes im-
 121 pact tracer transport at different scales. Our main finding is that the response of EKE
 122 and transport to changing winds is non-monotonic across scales, larger scales get stronger
 123 while smaller scales get weaker. We describe our model and analysis methods in section
 124 2, present our main results in section 3, and conclude with a discussion in section 4.

125 2 Model and Methods

126 2.1 Model and Experiment Description

127 This study uses the Massachusetts Institute of Technology general circulation model
 128 (MITgcm) (Marshall et al., 1997a, 1997b) to carry out two pairs of channel experiments
 129 forced by zonal winds and surface buoyancy restoring. The first pair configuration - chan-
 130 nel with flat topography - is similar to Abernathey et al. (2011), which demonstrated
 131 the validity of such channel configurations for studying the Southern Ocean. The domain
 132 is a square channel of size $2,000\text{km} \times 2,000\text{km} \times 4\text{km}$ on a β -plane (β is $1.4E^{-11}$) with
 133 a flat bottom. The southernmost Coriolis frequency is $-1.1E^{-4}$. The horizontal reso-
 134 lution is 5km, which is adequate for resolving mesoscale eddies. The vertical grid has 49
 135 levels with spacing increasing from 1 m at the surface to 200m at the bottom. At the
 136 surface boundary layer, we use the K-profile boundary layer parametrization (Large et
 137 al., 1994). Following Balwada et al. (2018), the numerical viscosity is set by the Mod-
 138 ified Leith Viscosity (Fox-Kemper & Menemenlis, 2008). The quadratic bottom drag co-
 139 efficient is 0.0021. A linear equation of seawater state that depends on temperature is
 140 used. Additionally, there is a linear temperature restoration at the surface, with the restora-
 141 tion temperature profile increasing from south to north.

142 Considering the importance of the bathymetric features in modulating the real ACC
 143 flows and EKE (Holloway, 1978; Thompson, 2010; Melet et al., 2013; Howard et al., 2015;
 144 Jouanno & Capet, 2020; Zhang et al., 2023), a second pair of experiments were conducted
 145 where a topographic ridge was introduced (Abernathey & Cessi, 2014; Balwada et al.,
 146 2018). These channel experiments also doubled the domain length, following the setup
 147 from Youngs et al. (2023), allowing us to distinguish more clearly between regions closer
 148 and away from the ridge. The other physical parameters and initial fields are the same
 149 as those in the flat channel.

150 Both sets of channel simulations were forced by wind stress with a sinusoidal pro-
 151 file, peaking in amplitude in the middle of the domain. The flat bottom experiments have
 152 a peak amplitude of $0.1N/m^2$ (FLAT-WIND10) and $0.3N/m^2$ (FLAT-WIND30), and
 153 the ridge experiments have peak amplitudes of $0.15N/m^2$ (RIDGE-WIND15) and $0.3N/m^2$
 154 (RIDGE-WIND30). This tripling and doubling of wind is an exaggeration of the actual
 155 wind change in the Southern Ocean, which increased by roughly 10% (Lin et al., 2018).
 156 However, this large amplification was used following previous studies, e.g. Abernathey
 157 et al. (2011); Abernathey and Ferreira (2015b), to clearly see the emerging changes. The
 158 change in the wind did not dramatically change the stratification, and the associated de-
 159 formation radius between the experiments was similar. All experiments were spun up
 160 for 50 years before further analysis.

161 2.2 The Eddy Kinetic Energy Budget

162 To understand the details of how the mesoscale turbulence changed in response to
 163 the winds, we considered the eddy kinetic energy (EKE) budget.

164 In zonally periodic domains, it is convenient to define the eddy field relative to the
 165 zonal mean. The eddy velocity is defined as $u' = u - \bar{u}$ where $\bar{u} = \frac{1}{L_x} \oint u dx$. When

166 there is no topography, the zonal mean can cleanly separate the zonal mean flow and the
 167 time-varying turbulence fields. While in the presence of topography, the variability in-
 168 cludes both the time-varying eddies and standing meanders.

169 The point-wise horizontal EKE ($EKE = 0.5(u'^2 + v'^2)$) budget equation can be
 170 constructed by taking the dot product of the horizontal eddy velocity ($U'_h = [u', v']$)
 171 with the horizontal eddy momentum equation. This results in,

$$\frac{\partial EKE}{\partial t} = -U'_h U' \cdot \nabla U'_h - U'_h \bar{U} \cdot \nabla U'_h - U'_h U' \cdot \nabla \bar{U}_h + U'_h \overline{U' \cdot \nabla U'_h} - \frac{1}{\rho_c} U'_h \cdot \nabla_h P' + U'_h \cdot \mathcal{F}'. \quad (1)$$

172 Here $U' = [u', v', w']$ is the 3D velocity, $U'_h = [u', v']$ is the horizontal velocity, $\nabla =$
 173 $(\partial_x, \partial_y, \partial_z)$ is the 3D gradient operator, $\nabla_H = (\partial_x, \partial_y)$ is the horizontal gradient op-
 174 erator, P' is the pressure perturbation, and \mathcal{F}' is the momentum forcing perturbation.

175 The first four terms on the right-hand side (RHS) are nonlinear terms relating to
 176 how eddies interact with each other and the mean flow. Here the first nonlinear term rep-
 177 represents eddy-eddy interactions (named as 'EEE'). The second and third nonlinear terms
 178 represent the eddy-mean interactions and are referred to as 'EME' and 'EEM' respec-
 179 tively. The fourth nonlinear term disappears after the zonal average. The fifth term is
 180 horizontal pressure work and the last term is the work by the variable forcing. It should
 181 be recognized that constant wind forcing does no direct work in the EKE budget, and
 182 so can not energize or kill eddies. Further, the horizontal pressure work is rewritten as:
 183 $-\frac{1}{\rho_c} U'_h \cdot \nabla_h P' = -\frac{1}{\rho_c} \nabla \cdot (U' P') + w' b'$. The first term integrates to zero in a domain
 184 average. $w' b'$ is usually a source of EKE associated with the baroclinic instability and
 185 represents the conversion of the eddy potential energy (EPE) to EKE.

186 Since this study focuses on the multi-scale nature of the EKE, we considered the
 187 scale-wise decomposition of this EKE budget averaged over time and the zonal direction.
 188 This scale-wise decomposition was done by analyzing the spectral EKE budget. Since
 189 our domain is a re-entrant channel, we only consider the zonal Fourier transform: $\hat{u}'(k) =$
 190 $\int u' e^{ikx} dx$. This obviates the need for any tapering and avoids any associated spectral
 191 contamination (Uchida et al., 2019; Schubert et al., 2020). In this spectral space, the hor-
 192 izontal EKE power spectrum is defined as $\hat{E}(\kappa) = 0.5(\hat{u}'^\dagger \hat{u}' + \hat{v}'^\dagger \hat{v}')$, where $(\hat{\cdot})$ and $(\cdot)^\dagger$
 193 represent the Fourier transform and its conjugate. Parseval's theorem implies that $\overline{EKE} =$
 194 $\sum_k \hat{E}(\kappa)$, suggesting that $\hat{E}(\kappa)$ decomposes the zonal mean EKE into wave components
 195 in different spatial scales. The equation for each of these spectral components can be de-
 196 rived in the same way as the equation for the EKE budget, by taking Fourier transforms
 197 of the velocity and eddy momentum equation. We used the Python package - xrft ([https://](https://xrft.readthedocs.io/)
 198 xrft.readthedocs.io/) for doing all the spectral analysis.

199 2.3 Tracer Experiments

200 To study the impact of changing winds on tracer transport, we conducted passive
 201 tracer experiments. These tracers were used to estimate the tracer fluxes, eddy diffusiv-
 202 ity, and spectral properties of tracer fluxes.

203 Since the multi-scale response of the spectral EKE to the wind forcing is more clear
 204 in the flat channel, we deployed four passive tracers with the following initial concen-
 205 tration profiles in the flat channel experiments:

$$C1 = y; C2 = z; C3 = \cos(\pi y/L_y) \cos(\pi z/H); C4 = \sin(\pi y/L_y) \sin(\pi z/H). \quad (2)$$

206 These tracers were initialized after the 50-year model spin-up and were evolved for
 207 3 years. Tracer statistics were computed using five-day snapshots from the third month
 208 after tracer initialization till the end of the 3 years.

209

2.4 The spectral decomposition of transport and eddy diffusivity

We investigated the scale-wise characteristics of the transport by assessing the cross-spectra of tracer fluxes (Balwada et al., 2018), which decomposes the meridional and vertical flux of tracers as

$$\overline{v'C'} = \sum_k \hat{v}'\hat{C}'^\dagger \quad (3)$$

$$\overline{w'C'} = \sum_k \hat{w}'\hat{C}'^\dagger, \quad (4)$$

210

and provides a sense of how different scales contribute to transport.

211

212

213

214

215

216

217

218

Since we compare multiple simulations with different forcing and different EKE levels, the evolution of the passive tracers will be different. So, the tracer flux patterns at any particular time may be impacted by the stage of the tracer evolution. To mitigate this and only compare the properties of transport related to the equilibrated flow and not related to the evolving tracer state we computed the eddy diffusivity. Further, the spectral eddy diffusivity is defined as the ratio of the cross-spectrum of the eddy transport to the background mean gradient of the passive tracer, as suggested by Kong and Jansen (2017). The formula is as follows:

$$D(\kappa) = -\frac{Re(\langle \hat{v}'\hat{C}'^\dagger \rangle)}{\partial \langle \bar{C} \rangle / \partial y} \quad (5)$$

219

220

Here the eddy transport and its corresponding mean gradient are calculated from the first tracer, C_1 , due to its initial meridional gradient. $\langle \cdot \rangle$ represents the time mean.

221

222

223

224

225

226

227

228

229

Some recent studies estimated the full diffusivity tensor, to relate the eddy tracer flux to its mean gradients (Bachman et al., 2015; Abernathey et al., 2013; Balwada et al., 2019). We also diagnosed this diffusivity tensor, which is why we deployed four tracers in tracer experiments. However, we found that the meridional diffusivity estimated using only the meridional flux and meridional gradient is the same as the major eigenvalue of the diffusivity tensor, which is oriented primarily in the meridional direction. The correlation coefficient of the diffusivity between the two methods is 0.9989 (0.9914) in the FLAT-WIND10 (FLAT-WIND30). Thus, we decided to only present results from the analysis using the simpler estimate of only meridional eddy diffusivity.

230

231

232

233

We expect the transport properties, quantified in terms of scale-wise diffusivity, to be related to the levels of EKE as a function of scale. One derivation of such a relationship was presented in Kong and Jansen (2017). Based on a barotropic beta plane model, they related the diffusivity to the energy spectrum as follows:

$$D = \int_0^\infty D(\kappa) d\kappa = \frac{1}{C_1} \int_0^\infty \frac{E(\kappa)^{\frac{1}{2}} \kappa^{-\frac{3}{2}}}{1 + \frac{C_2 \beta^2}{2C_1^2 E(\kappa) \kappa^5}} d\kappa \quad (6)$$

234

235

236

237

238

239

240

241

$E(\kappa)$ is the EKE spectrum and κ is the wave number. The two parameters, C_1 and C_2 are empirical parameters, which can be obtained by the least squares fitting. In this study, we estimated these parameters using the FLAT-WIND10 and found that $C_1 = 1.2E^{-3}$ and $C_2 = 9.5E^{-9}$ respectively. We also used this formula and the estimated parameters to predict the scale-dependent diffusivity in the FLAT-WIND30 and found that there was a good agreement - suggesting that the formula works well and the parameters are not very sensitive to the range of flow regimes. We use this formulation to suggest that transport changes are primarily a result of the changes in the energy spectrum.

242

3 Results

243

244

As discussed in the introduction, our observational analysis of the changes in the geostrophic EKE in many sectors of the ACC (sufficiently far away from topography)

245 found a robust enhancement of larger-scale EKE ($> 180\text{km}$), accompanied by a suppression
 246 of smaller mesoscale EKE ($90 - 180\text{km}$) (Figure 1a and Figure S5). This should
 247 be viewed in the context of the well-documented acceleration of ACC jets and enhanced
 248 total EKE (A. M. Hogg et al., 2015; Shi et al., 2021). To understand the dynamics and
 249 implications of the non-monotonic changes in the EKE across scales, we analyze the response
 250 of the EKE spectrum in two pairs of experiments.

251 3.1 The Weakened Smaller-Scale Mesoscale Eddy Kinetic Energy

252 First, we describe the results from the flat bottom simulations, which are much more
 253 qualitatively aligned with the satellite observations. Consistent with previous studies (Abernathey
 254 et al., 2011; Abernathey & Ferreira, 2015b), the stronger wind forcing results in a stronger
 255 zonal mean flow and EKE (Figure 1b), particularly in the middle of the domain ($500-$
 256 1500km). However, these previous studies have not considered how the EKE changes across
 257 different scales. We find that the response of the EKE at different wavenumbers to the
 258 strengthened wind is non-monotonic and not the same as the response of the total EKE.
 259 The surface EKE spectrum, Figure 1c, shows that the surface EKE increases at scales
 260 larger than $\sim 250\text{km}$ and decreases at scales smaller than $\sim 250\text{km}$ in the region when
 261 the stronger winds drive the stronger zonal jet. The relative change in energy ($\frac{EKE_{30}-EKE_{10}}{EKE_{10}}$)
 262 at the large scales is about a factor of 1.29, while the relative change at smaller scales
 263 is about a factor of -0.46 (Figure 1c). In addition, the scale below which the EKE is sup-
 264 pressed (above which the EKE is enhanced) remains roughly constant with depth, de-
 265 creasing very slightly from 267km at the surface to about 227km at 500m (Figure S3).

266 The scale-wise EKE budgets are useful to investigate the physical processes that
 267 result in the scale-wise eddy response to the wind forcing. Here, we consider the terms
 268 in the spectral EKE budget corresponding to the conversion of the EPE to EKE ($\overline{w'b'}$),
 269 the transfer of kinetic energy due to the eddy-mean interaction (EME and EEM), and
 270 the transfer of EKE due to the eddy-eddy interaction (EEE). Figure 1d shows the four
 271 terms vertically averaged over the upper 500m , negative values indicate EKE loss, and
 272 positive values indicate EKE gain. Generally, the baroclinic instability results in a con-
 273 version of EPE to EKE, which results in a peak near $\sim 250\text{km}$ in these simulations. The
 274 largest contributor to the EKE loss near the same scales is the EEE. The EEE also in-
 275 creases the EKE at larger scales, which in combination with the smaller scale energy loss
 276 is associated with the inverse energy cascade (Scott & Wang, 2005; Schubert et al., 2020)
 277 - transferring the smaller-scale mesoscale EKE to the larger scales. The EEM is smaller
 278 than the EEE and does not contribute individually to the inverse energy transfer. The
 279 residuals of these four terms are balanced by the pressure work and dissipation.

280 When the wind forcing is strengthened, there are subtle changes in the aforemen-
 281 tioned balance (Figure 1d). Generally, the intensification of EEE and EEM contributes
 282 to a greater loss of EKE in the mesoscales and very slight increase at larger scales. Fur-
 283 thermore, the replenishment of mesoscale EKE by the $\overline{w'b'}$ does not show any signifi-
 284 cant increase in strength. However, it does shift slightly towards larger scales. This shift
 285 results in an increased conversion of available eddy potential energy (EPE) to EKE at
 286 scales larger than approximately 250 km , while the conversion decreases at scales smaller
 287 than the same scales. Additionally, the peaks of EEE and EEM also exhibit a slight shift
 288 towards larger scales. It is worth noting that a similar shift towards larger scales in spec-
 289 tral energy budgets has been recently reported for atmospheric flows by (Chemke & Ming,
 290 2020). They found that under changing zonal mean wind and stratification induced by
 291 climate change, larger atmospheric waves become stronger while smaller waves become
 292 weaker in mid-latitudes.

293 The experiments with the ridge, Figure 1e, illustrate similar non-monotonic changes
 294 of the EKE spectrum in the region 2000km downstream of the ridge. However, the scale
 295 where the EKE begins to be suppressed is substantially reduced to a wavenumber of 40km ,

296 and the suppression is much weaker compared to that in the flat channel. The spectral
 297 EKE budgets suggest that the weaker mesoscale suppression phenomenon in the ridge
 298 case is mainly due to a significant increase in baroclinic eddy energy source $w'b'$ at all
 299 scales under intensified westerly (Figure 1f). This increase counteracts the reduction of
 300 mesoscale EKE caused by EEE and EEM.

301 These flat and ridge channels are only idealized analogs for the Southern Ocean,
 302 and are not designed to perfectly capture the scales of observed changes, but rather show
 303 that wind changes alone can qualitatively describe the observed changes in the EKE at
 304 different scales. This initial foray, suggests that the dynamics of actual ACC regions away
 305 from topography may lie somewhere between the flat and ridge channels explored here,
 306 and more work including more realistic domains and forcing would be needed for quan-
 307 titative investigation.

308 **3.2 The Suppressed Mesoscale Eddy Transport and Diffusivity**

309 Many previous studies found that eddies play a major role in the meridional trans-
 310 port across the ACC (Volkov et al., 2008; Dufour et al., 2015), and this transport is likely
 311 to increase as winds strengthen (A. M. C. Hogg et al., 2008; Spence et al., 2010; Aber-
 312 nathey & Ferreira, 2015b). We expect the same net result in our simulations since the
 313 net EKE does increase with increasing winds. In the context of the multiscale response
 314 of the spectral EKE to the wind forcing, we consider how the scale-wise eddy transport
 315 changes only in the flat channel.

316 Here we focus on the depth-averaged eddy transport, as there are no significant ver-
 317 tical changes in the EKE and eddy transport (Figure S3). Figure 2 shows the cross-spectrum
 318 of the meridional, the vertical eddy transport, and the meridional component of the EKE
 319 spectrum. In both experiments, the peak of the meridional eddy transport primarily oc-
 320 curs on scales around 430km within the strong zonal flow (500-1500km), owing to the
 321 relatively high EKE levels. Comparing the two experiments, we find that the eddy trans-
 322 port is suppressed in the FLAT-WIND30 for scales smaller than ~ 430 km but is increased
 323 for scales larger than ~ 430 km. This result can be attributed to the suppression of smaller
 324 mesoscale EKE and enhancement of larger-scale EKE. However, the scales at which the
 325 eddy transport is suppressed do not perfectly align with the scales where EKE reduc-
 326 tion occurs. The cross-over scale for transport is ~ 430 km, whereas the cross-over scale
 327 for the energy spectrum is slightly smaller ~ 250 km.

328 Similar to the response of the meridional transport, the vertical transport also shows
 329 a non-monotonic response. The qualitative scale-wise vertical transport is different be-
 330 tween the two experiments; while most scales are associated with upwelling in FLAT-
 331 WIND10, the vertical transport in FLAT-WIND30 changes sign with scale (the net re-
 332 sult is still upwelling). Also, the strengthened wind forcing significantly enhances the up-
 333 welling transport on scales larger than ~ 430 km and moderately enhances the downwelling
 334 transport on scales ranging from 120 km to 430km. These changes correspond to the dif-
 335 ferent increases in the vertical component of EKE at each scale (not shown). Although
 336 the model in this study is only mesoscale resolving and has a weak vertical motion, the
 337 different transport directions in different scales may have important implications on bio-
 338 geochemistry and should be considered in higher-resolution simulations in the future.

339 The cross-spectrum of eddy transport can be utilized to evaluate the spectral mesoscale
 340 eddy diffusivity through equation 4 and further probe the properties of the transport.
 341 The pattern of the meridional spectral diffusivity depends mainly on the cross-spectrum
 342 of eddy transport (Figure 2). Consequently, the peak of spectral diffusivity also occurs
 343 mostly on scales ~ 430 km. In addition, the mesoscale diffusivity is also suppressed at scales
 344 of less than ~ 430 km. This feature serves as a valuable indicator for evaluating scale-dependent
 345 diffusivity theories. Figure 2m and 2n show the spectral diffusivity predicted by the dif-
 346 fusivity spectrum theory proposed by (Kong & Jansen, 2017). The correlation coefficient

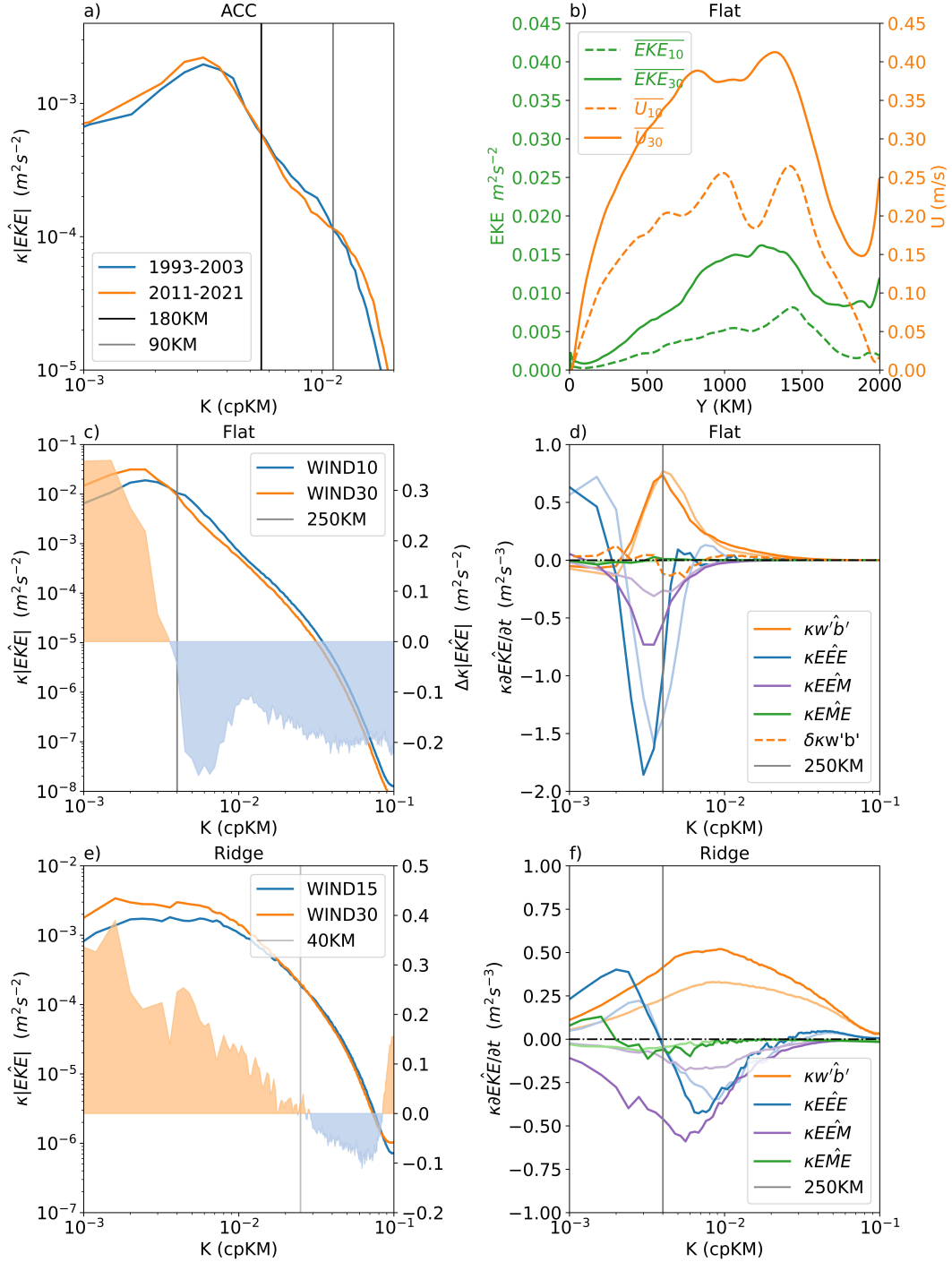


Figure 1. a), The ten-year averaged variance-preserving geostrophic EKE zonal spectrum in the jet region (50°S - 45°S) of the ACC Atlantic Section (320°E - 360°E) as seen in Figure S5a. The unit is m^2/s^2 . b), The zonal and vertical mean zonal velocity and the EKE in the two experiments, where the solid (dashed) lines represent the FLAT-WIND30 (FLAT-WIND10) experiment. The X-axis is the south-north direction in km. The unit of zonal velocity and EKE is m/s and m^2/s^2 . c), The meridional averaged variance preserving the EKE spectrum from 500km to 1500km in the two experiments. The unit is m^2/s^2 . The orange and blue color shadings indicate the increased and suppressed EKE at each wavenumber, respectively. d), The variance preserving spectral $w'b'$, EEM , EME , and EEE which are meridionally averaged from 500km to 1500km over the upper 500m in the FLAT-WIND10 (light colors) and FLAT-WIND30 (dark colors). The unit is $10^{-9}m^2/s^3$. The orange dashed line shows the difference of the $w'b'$ between the FLAT-WIND30 and the FLAT-WIND10. The unit is m^2/s^3 . e), the same as 1c, but for the variance preserving EKE spectrum from 250km to 1100km in the downstream ridge regions, since the latitude positions of the southern branches of the downstream zonal jet are relatively stable, in contrast to the northern branches. f), the same as 1d, but for the two downstream ridge regions.

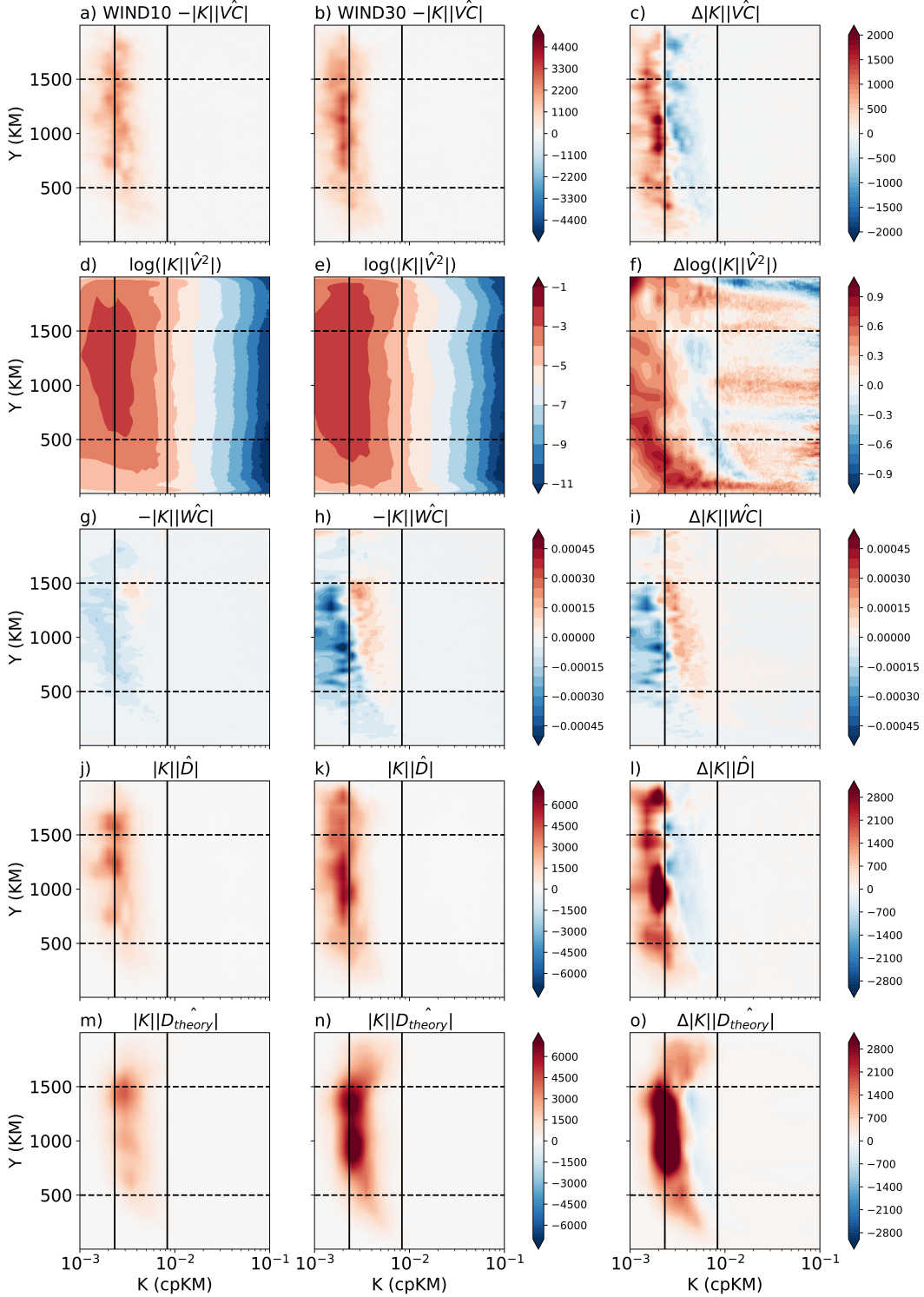


Figure 2. a), The cross-spectrum of the meridional eddy transport in the FLAT-WIND10. The unit is m/s . b), the same as a) but for the FLAT-WIND30. c), the difference in the cross-spectrum of the meridional eddy transport between the two experiments. d), the meridional component of the variance preserving EKE spectrum in the FLAT-WIND10. The unit is $\log_{10} m^2/s^2$. e), the same as 2d but for the FLAT-WIND30. f), the difference in the EKE spectrum between the two experiments. g) The cross-spectrum of the vertical eddy transport in the FLAT-WIND10. The unit is m/s . h), the same as 2g but for the FLAT-WIND30. i), the difference in the cross-spectrum of the vertical eddy transport between the two experiments. j), the diagnosed spectral diffusivity in the FLAT-WIND10. The unit is $\kappa \times m^2 s^{-1}$. k), the same as 2j but for the FLAT-WIND30. l), the difference in the spectral diffusivity between the two experiments. m) theoretical diffusivity in the FLAT-WIND10. The unit is $m^2 s^{-1}$. n), the same as 2m but for the FLAT-WIND30. o), the difference in the theoretical diffusivity between the two experiments. The two solid lines in each figure are the wavelengths at 430km and 120km from left to right. The X-axis is the wavenumber, whose unit is km^{-1} . The Y-axis is the cross-frontal

347 between the integral of the diagnosed and theoretical spectral diffusivity are 0.8890 (FLAT-
 348 WIND10) and 0.9356 (FLAT-WIND30) along the meridional direction. In the spectral
 349 space, the theory succeeds in predicting the suppressed mesoscale diffusivity as well. This
 350 suggests that considering the EKE spectrum, rather than the total EKE, could be ben-
 351 efiticial for parameterizing mesoscale diffusivity in the ocean. It should be noted, that the
 352 scale of the theoretical suppressed diffusivity peaks at a slightly smaller scale compared
 353 with the diagnosed spectral diffusivity. This is because theoretically, the eddy diffusiv-
 354 ity is a direct response to the EKE spectrum, thus making the scale of the predicted dif-
 355 fusivity peak dependent on the EKE spectrum peak, while the actual response is slightly
 356 different from this theory. This suggests a need to maybe introduce different efficiency
 357 of stirring at different scales. However, this investigation is beyond the scope of this work
 358 and will be investigated in future theoretical studies.

359 4 Discussion and Conclusions

360 The Southern Ocean westerly winds have strengthened over the past few decades.
 361 Some recent studies have explored the response of the ocean eddies to the strengthen-
 362 ing winds and found that the EKE is increasing. However, none of these studies have
 363 tried to investigate whether the EKE is increasing across all scales, or if the EKE at dif-
 364 ferent scales is responding differently to the changing winds. We found the observed multi-
 365 scale response of the geostrophic EKE to the changing winds is non-monotonic in regions
 366 far away from the topographic ridges. We investigated this multi-scale response of the
 367 EKE through idealized channel simulations forced with different wind amplitudes.

368 Our simulations, similar to past studies, show that the EKE increases as winds strengthen.
 369 However, this EKE response is not uniform across spatial scales. In simulations with flat
 370 topography, we find that the mesoscale eddies smaller than ~ 250 km are weakened, while
 371 the larger eddies are strengthened. In these simulations, this response is the strongest
 372 in the top 500m of the domain. It is also worth noting that the scale where the EKE change
 373 switches from strengthening to weakening is not fixed, as it can vary depending on dif-
 374 ferent parameters related to the source of eddy energy, including bathymetric features
 375 and buoyancy forcings. In the simulations of a ridge, the scales at which the suppres-
 376 sion of EKE begins can be significantly reduced to 40 km. Conversely, the scales are ex-
 377 panded to ~ 320 km when the surface buoyancy restoration was turned off (not shown
 378 here).

379 The EKE's non-monotonic response at different scales can likely be linked to non-
 380 monotonic changes in the spectral EKE budget. In the flat channel, the stronger zonal
 381 jet intensifies eddy-eddy (EEE) and eddy-mean (EEM) interactions, reducing smaller
 382 mesoscale EKE and increasing larger-scale EKE, suggesting an intensified inverse kinetic
 383 energy cascade. Additionally, the EKE generation also shifts slightly towards larger scales,
 384 contributing to the EKE spectrum's non-monotonic response. In the presence of a ridge,
 385 although the strengthened EEE and EEM similarly transfer more EKE into larger scales
 386 under stronger wind forcing, a significant increase in the baroclinic EKE source coun-
 387 teracts the reduction of smaller-scale mesoscale EKE through the inverse cascade pro-
 388 cesses. As a result, the phenomenon of mesoscale EKE suppression is weakened. Based
 389 on these simulations, it is plausible that the actual ACC falls somewhere between the
 390 scenarios of the flat and the ridge channel, since the observed suppression of EKE oc-
 391 curs within the scale range of approximately 180km to 90km.

392 These non-monotonic changes in the scale-wise statistics may be linked mechanis-
 393 tically to the change in the zonal flow under changing winds. Liu et al. (2022) showed,
 394 using both observations and simulations, that stronger jets and zonal flows result in a
 395 more rapid loss of eddy energy and shortened eddy lifetime, as this eddy energy is more
 396 efficiently converted to larger-scale Rossby waves. In our simulations, the zonal flow speeds
 397 up by about 40-50% as the wind strength triples, which could result in a more efficient

398 conversion of kinetic energy from mesoscale eddies to larger Rossby waves. These processes
399 can be seen by considering the flow structure at different scales. In Figure S4, we
400 show that the simulation with stronger winds has more energetic features at larger scales
401 with meridionally elongated bow-type shapes, which are generally associated with Rossby
402 waves (Early et al., 2011). This enhancement of large-scale wave-like structures comes
403 at the expense of smaller relatively isotropic eddies. This hypothesis is also quantitatively
404 supported by considering the eddy lifetimes, which show that there are significantly fewer
405 mesoscale eddy tracks with longer lifetimes in the FLAT-WIND30 compared to those
406 in the FLAT-WIND10 (Figure S1 and S2).

407 In summary, the non-monotonic multiscale response of the EKE to the strengthened
408 wind is not trivial but reflects some profound changes in physical processes on different
409 scales. The inverse kinetic energy cascade and the zonal mean flow "killing" smaller-
410 scale mesoscale eddies and facilitating the larger-scale wave activity are the potential mechanisms
411 that lead to the non-monotonic multi-scale responses.

412 Since the stirring by mesoscale eddies dominates the eddy transport of passive tracers
413 (Klocker & Abernathey, 2014), the non-monotonic multi-scale response of the EKE
414 has important implications for eddy transport and diffusivity. We investigated the detailed
415 properties of eddy transport by considering the cross-spectra of passive tracer flux
416 and the spectral eddy diffusivity. The cross-spectrum of the meridional eddy flux confirmed
417 the suppression (amplification) of turbulent transport at the smaller (larger) scales
418 in the stronger winds. Additionally, we showed that vertical transport also responds non-
419 monotonically to these changes, with the smaller scales starting to oppose the transport
420 by the larger-scale eddies in the stronger wind. This may have non-trivial implications
421 for the biogeochemical tracers, where the time scale of tracer transport and its interactions
422 with different reaction time scales can lead to complex system responses (Freilich
423 et al., 2022).

424 Further, since the cross-spectrum of the meridional eddy transport is related to the
425 spectral eddy diffusivity, the eddy diffusivity is also enhanced at larger scales but is suppressed
426 at smaller scales. The theoretical formula for scale-dependent diffusivity, derived
427 by Kong and Jansen (2017), generally succeeds in predicting the eddy diffusivity, suggesting
428 that the response of the transport to changing winds is largely linked to changes
429 in the EKE spectrum. This suggests that it is possible to build transport parameterizations
430 for the effects seen in this study by linking the diffusivity to the EKE spectrum,
431 as long as the appropriate EKE spectrum response to changing winds is achieved.

432 This study is the first to consider the multiscale response of ocean mesoscale eddies
433 to changes in the wind forcing and leaves much room for further investigations into
434 the nature of the eddy response. Future research could utilize more realistic ocean general
435 circulation models to investigate the responses of multi-scale Southern Ocean eddies
436 to surface forcings under climate change in the actual ocean basins. Additionally,
437 while this study focused on mesoscale-resolving processes, it is also important to investigate
438 the role of sub-mesoscale processes in shaping the response of smaller-scale EKE
439 to forcings. Such investigations would contribute to a more comprehensive understanding
440 of ocean eddies' multiscale dynamics and behavior.

441 5 Open Research

442 The data used in this study are mainly generated through the model. The model
443 configurations to regenerate the high-frequency output data used in this study and the
444 figures' scripts with the data to produce the figures can be obtained from Ran (2023)
445 . Additionally, the observational geostrophic EKE spectrum data used for analysis in this
446 study were obtained from the delayed-time altimeter gridded products provided by E.U
447 Copernicus Marine Service Information, Marine Data Store (2023). Figures were plot-

448 ted by using the Python package Matplotlib (The Matplotlib Development Team, 2023).
 449 The wavenumber spectra in this study is calculated by using the Python package xrft
 450 (Uchida et al., 2023). The mesoscale eddy identification is through the Python package
 451 py-eddy-tracker (Delepuolle et al., 2022).

452 Acknowledgments

453 RL and GW were supported by the National Natural Science Foundation of China (42030405;
 454 42288101). DB was supported by NSF-OCE-2242110. We truly appreciate the insight-
 455 ful suggestions from two anonymous reviewers and Prof. Andy Hogg that helped enhance
 456 the quality of the paper.

457 References

- 458 Abernathey, R., & Cessi, P. (2014). Topographic enhancement of eddy efficiency in
 459 baroclinic equilibration. *Journal of physical oceanography*, *44*(8), 2107–2126.
- 460 Abernathey, R., & Ferreira, D. (2015b). Southern ocean isopycnal mixing and venti-
 461 lation changes driven by winds. *Geophysical Research Letters*, *42*(23), 10–357.
- 462 Abernathey, R., Ferreira, D., & Klocker, A. (2013). Diagnostics of isopycnal mixing
 463 in a circumpolar channel. *Ocean Modelling*, *72*, 1–16.
- 464 Abernathey, R., Marshall, J., & Ferreira, D. (2011). The dependence of southern
 465 ocean meridional overturning on wind stress. *Journal of Physical Oceanogra-
 466 phy*, *41*(12), 2261–2278.
- 467 Bachman, S. D. (2019). The gm+ e closure: A framework for coupling backscat-
 468 ter with the gent and mcwilliams parameterization. *Ocean Modelling*, *136*, 85–
 469 106.
- 470 Bachman, S. D., Fox-Kemper, B., & Bryan, F. O. (2015). A tracer-based inver-
 471 sion method for diagnosing eddy-induced diffusivity and advection. *Ocean
 472 Modelling*, *86*, 1–14.
- 473 Balwada, D., Smith, K. S., & Abernathey, R. (2018). Submesoscale vertical veloc-
 474 ities enhance tracer subduction in an idealized antarctic circumpolar current.
 475 *Geophysical Research Letters*, *45*(18), 9790–9802.
- 476 Balwada, D., Smith, K. S., & Abernathey, R. P. (2019). Measuring eddy driven
 477 transport in a zonally inhomogeneous flow. In *22nd conference on atmospheric
 478 and oceanic fluid dynamics*.
- 479 Balwada, D., Xie, J.-H., Marino, R., & Feraco, F. (2022). Direct observational ev-
 480 idence of an oceanic dual kinetic energy cascade and its seasonality. *Science
 481 Advances*, *8*(41), eabq2566.
- 482 Barkan, R., Winters, K. B., & Smith, S. G. L. (2015). Energy cascades and loss
 483 of balance in a reentrant channel forced by wind stress and buoyancy fluxes.
 484 *Journal of Physical Oceanography*, *45*(1), 272–293.
- 485 Beech, N., Rackow, T., Semmler, T., Danilov, S., Wang, Q., & Jung, T. (2022).
 486 Long-term evolution of ocean eddy activity in a warming world. *Nature cli-
 487 mate change*, *12*(10), 910–917.
- 488 Busecke, J. J., & Abernathey, R. P. (2019). Ocean mesoscale mixing linked to cli-
 489 mate variability. *Science Advances*, *5*(1), eaav5014.
- 490 Buzzicotti, M., Storer, B., Khatri, H., Griffies, S., & Aluie, H. (2023). Spatio-
 491 temporal coarse-graining decomposition of the global ocean geostrophic
 492 kinetic energy. *Journal of Advances in Modeling Earth Systems*, *15*(6),
 493 e2023MS003693.
- 494 Chelton, D. B., Schlax, M. G., & Samelson, R. M. (2011). Global observations of
 495 nonlinear mesoscale eddies. *Progress in oceanography*, *91*(2), 167–216.
- 496 Chemke, R., & Ming, Y. (2020). Large atmospheric waves will get stronger, while
 497 small waves will get weaker by the end of the 21st century. *Geophysical Re-
 498 search Letters*, *47*(22), e2020GL090441.

- 499 Delepouille, A., evanmason, Clément, CoriPegliasco, Capet, A., Troupin, C., &
500 Koldunov, N. (2022). *Antsimi/py-eddy-tracker (v3.6.1)*. [software]. Zenodo.
501 Retrieved from <https://doi.org/10.5281/zenodo.7197432>
- 502 Dufour, C. O., Griffies, S. M., de Souza, G. F., Frenger, I., Morrison, A. K., Palter,
503 J. B., ... others (2015). Role of mesoscale eddies in cross-frontal transport
504 of heat and biogeochemical tracers in the southern ocean. *Journal of Physical*
505 *Oceanography*, *45*(12), 3057–3081.
- 506 Durack, P. J., Wijffels, S. E., & Matear, R. J. (2012). Ocean salinities reveal strong
507 global water cycle intensification during 1950 to 2000. *science*, *336*(6080), 455–
508 458.
- 509 Early, J. J., Samelson, R., & Chelton, D. B. (2011). The evolution and propagation
510 of quasigeostrophic ocean eddies. *Journal of Physical Oceanography*, *41*(8),
511 1535–1555.
- 512 Ellwood, M. J., Strzepek, R. F., Strutton, P. G., Trull, T. W., Fourquez, M., &
513 Boyd, P. W. (2020). Distinct iron cycling in a southern ocean eddy. *Nature*
514 *Communications*, *11*(1), 825.
- 515 E.U Copernicus Marine Service Information, Marine Data Store. (2023). *Global*
516 *ocean gridded 1/4 sea surface heights and derived variables reprocessed coperni-*
517 *cus climate service*. [Dataset]. Retrieved from [https://doi.org/10.48670/](https://doi.org/10.48670/moi-00145)
518 [moi-00145](https://doi.org/10.48670/moi-00145)
- 519 Fox-Kemper, B., & Menemenlis, D. (2008). Can large eddy simulation techniques
520 improve mesoscale rich ocean models? *Washington DC American Geophysical*
521 *Union Geophysical Monograph Series*, *177*, 319–337.
- 522 Freilich, M. A., Flierl, G., & Mahadevan, A. (2022). Diversity of growth rates max-
523 imizes phytoplankton productivity in an eddying ocean. *Geophysical Research*
524 *Letters*, *49*(3), e2021GL096180.
- 525 Frenger, I., Münnich, M., & Gruber, N. (2018). Imprint of southern ocean mesoscale
526 eddies on chlorophyll. *Biogeosciences*, *15*(15), 4781–4798.
- 527 Garabato, A. C. N., Yu, X., Callies, J., Barkan, R., Polzin, K. L., Frajka-Williams,
528 E. E., ... Griffies, S. M. (2022). Kinetic energy transfers between mesoscale
529 and submesoscale motions in the open ocean’s upper layers. *Journal of Physi-*
530 *cal Oceanography*, *52*(1), 75–97.
- 531 Gnanadesikan, A., Pradal, M.-A., & Abernathey, R. (2015). Isopycnal mixing by
532 mesoscale eddies significantly impacts oceanic anthropogenic carbon uptake.
533 *Geophysical Research Letters*, *42*(11), 4249–4255.
- 534 Griffies, S. M., Winton, M., Anderson, W. G., Benson, R., Delworth, T. L., Dufour,
535 C. O., ... others (2015). Impacts on ocean heat from transient mesoscale
536 eddies in a hierarchy of climate models. *Journal of Climate*, *28*(3), 952–977.
- 537 Haumann, F. A., Gruber, N., Münnich, M., Frenger, I., & Kern, S. (2016). Sea-
538 ice transport driving southern ocean salinity and its recent trends. *Nature*,
539 *537*(7618), 89–92.
- 540 Hogg, A. M., Meredith, M. P., Chambers, D. P., Abrahamsen, E. P., Hughes, C. W.,
541 & Morrison, A. K. (2015). Recent trends in the southern ocean eddy field.
542 *Journal of Geophysical Research: Oceans*, *120*(1), 257–267.
- 543 Hogg, A. M. C., Meredith, M. P., Blundell, J. R., & Wilson, C. (2008). Eddy heat
544 flux in the southern ocean: Response to variable wind forcing. *Journal of Cli-*
545 *mate*, *21*(4), 608–620.
- 546 Holloway, G. (1978). A spectral theory of nonlinear barotropic motion above irregu-
547 lar topography. *Journal of Physical Oceanography*, *8*(3), 414–427.
- 548 Howard, E., Hogg, A. M., Waterman, S., & Marshall, D. P. (2015). The injection of
549 zonal momentum by buoyancy forcing in a southern ocean model. *Journal of*
550 *Physical Oceanography*, *45*(1), 259–271.
- 551 Jansen, M. F., & Held, I. M. (2014). Parameterizing subgrid-scale eddy effects using
552 energetically consistent backscatter. *Ocean Modelling*, *80*, 36–48.
- 553 Jouanno, J., & Capet, X. (2020). Connecting flow–topography interactions, vorticity

- 554 balance, baroclinic instability and transport in the southern ocean: the case of
 555 an idealized storm track. *Ocean Science*, 16(5), 1207–1223.
- 556 Klein, P., Lapeyre, G., Siegelman, L., Qiu, B., Fu, L.-L., Torres, H., . . . Le Gentil, S.
 557 (2019). Ocean-scale interactions from space. *Earth and Space Science*, 6(5),
 558 795–817.
- 559 Klocker, A., & Abernathey, R. (2014). Global patterns of mesoscale eddy properties
 560 and diffusivities. *Journal of Physical Oceanography*, 44(3), 1030–1046.
- 561 Kong, H., & Jansen, M. F. (2017). The eddy diffusivity in barotropic β -plane turbu-
 562 lence. *Fluids*, 2(4), 54.
- 563 Large, W. G., McWilliams, J. C., & Doney, S. C. (1994). Oceanic vertical mixing: A
 564 review and a model with a nonlocal boundary layer parameterization. *Reviews*
 565 *of geophysics*, 32(4), 363–403.
- 566 Lin, X., Zhai, X., Wang, Z., & Munday, D. R. (2018). Mean, variability, and trend
 567 of southern ocean wind stress: Role of wind fluctuations. *Journal of Climate*,
 568 31(9), 3557–3573.
- 569 Liu, R., Wang, G., Chapman, C., & Chen, C. (2022). The attenuation effect of jet
 570 filament on the eastward mesoscale eddy lifetime in the southern ocean. *Jour-*
 571 *nal of Physical Oceanography*, 52(5), 805–822.
- 572 Marshall, J., Adcroft, A., Hill, C., Perelman, L., & Heisey, C. (1997a). A finite-
 573 volume, incompressible navier stokes model for studies of the ocean on parallel
 574 computers. *Journal of Geophysical Research: Oceans*, 102(C3), 5753–5766.
- 575 Marshall, J., Hill, C., Perelman, L., & Adcroft, A. (1997b). Hydrostatic, quasi-
 576 hydrostatic, and nonhydrostatic ocean modeling. *Journal of Geophysical Re-*
 577 *search: Oceans*, 102(C3), 5733–5752.
- 578 Martínez-Moreno, J., Hogg, A. M., England, M. H., Constantinou, N. C., Kiss,
 579 A. E., & Morrison, A. K. (2021). Global changes in oceanic mesoscale currents
 580 over the satellite altimetry record. *Nature Climate Change*, 11(5), 397–403.
- 581 Melet, A., Nikurashin, M., Muller, C., Falahat, S., Nycander, J., Timko, P. G., . . .
 582 Goff, J. A. (2013). Internal tide generation by abyssal hills using analytical
 583 theory. *Journal of Geophysical Research: Oceans*, 118(11), 6303–6318.
- 584 Morrow, R., Ward, M. L., Hogg, A. M., & Pasquet, S. (2010). Eddy response to
 585 southern ocean climate modes. *Journal of Geophysical Research: Oceans*,
 586 115(C10).
- 587 Patara, L., Böning, C. W., & Biastoch, A. (2016). Variability and trends in south-
 588 ern ocean eddy activity in 1/12 ocean model simulations. *Geophysical Research*
 589 *Letters*, 43(9), 4517–4523.
- 590 Rai, S., Hecht, M., Maltrud, M., & Aluie, H. (2021). Scale of oceanic eddy killing by
 591 wind from global satellite observations. *Science Advances*, 7(28), eabf4920.
- 592 Ran. (2023). *liu-ran/multiscale_response_codes (v1.0.0)*. [software]. Zenodo. Re-
 593 trieved from <https://doi.org/10.5281/zenodo.10260678>
- 594 Rintoul, S. R. (2018). The global influence of localized dynamics in the southern
 595 ocean. *Nature*, 558(7709), 209–218.
- 596 Schubert, R., Gula, J., Greatbatch, R. J., Baschek, B., & Biastoch, A. (2020). The
 597 submesoscale kinetic energy cascade: Mesoscale absorption of submesoscale
 598 mixed layer eddies and frontal downscale fluxes. *Journal of Physical Oceanog-*
 599 *raphy*, 50(9), 2573–2589.
- 600 Scott, R. B., & Wang, F. (2005). Direct evidence of an oceanic inverse kinetic en-
 601 ergy cascade from satellite altimetry. *Journal of Physical Oceanography*, 35(9),
 602 1650–1666.
- 603 Shi, J.-R., Talley, L. D., Xie, S.-P., Peng, Q., & Liu, W. (2021). Ocean warming and
 604 accelerating southern ocean zonal flow. *Nature Climate Change*, 11(12), 1090–
 605 1097.
- 606 Siedler, G., Griffies, S., Gould, J., & Church, J. (2013). *Ocean circulation and cli-*
 607 *mate: a 21st century perspective*. Academic Press.

- 608 Smith, K. S., & Marshall, J. (2009). Evidence for enhanced eddy mixing at mid-
609 depth in the southern ocean. *Journal of Physical Oceanography*, *39*(1), 50–69.
- 610 Spence, P., Fyfe, J. C., Montenegro, A., & Weaver, A. J. (2010). Southern ocean
611 response to strengthening winds in an eddy-permitting global climate model.
612 *Journal of Climate*, *23*(19), 5332–5343.
- 613 Stammer, D., Wunsch, C., & Ueyoshi, K. (2006). Temporal changes in ocean eddy
614 transports. *Journal of Physical Oceanography*, *36*(3), 543–550.
- 615 Storer, B. A., Buzzicotti, M., Khatri, H., Griffies, S. M., & Aluie, H. (2022). Global
616 energy spectrum of the general oceanic circulation. *Nature communications*,
617 *13*(1), 5314.
- 618 Swart, N., & Fyfe, J. C. (2012). Observed and simulated changes in the south-
619 ern hemisphere surface westerly wind-stress. *Geophysical Research Letters*,
620 *39*(16).
- 621 The Matplotlib Development Team. (2023). *Matplotlib: Visualization with python*
622 *(v3.8.2)*. [software]. Zenodo. Retrieved from [https://doi.org/10.5281/](https://doi.org/10.5281/zenodo.10150955)
623 [zenodo.10150955](https://doi.org/10.5281/zenodo.10150955)
- 624 Thompson, A. F. (2010). Jet formation and evolution in baroclinic turbulence with
625 simple topography. *Journal of Physical Oceanography*, *40*(2), 257–278.
- 626 Thompson, A. F., & Sallée, J.-B. (2012). Jets and topography: Jet transitions and
627 the impact on transport in the antarctic circumpolar current. *Journal of physical*
628 *Oceanography*, *42*(6), 956–972.
- 629 Torres, H. S., Klein, P., Wang, J., Wineteer, A., Qiu, B., Thompson, A. F., ...
630 others (2022). Wind work at the air-sea interface: a modeling study in an-
631 ticipation of future space missions. *Geoscientific Model Development*, *15*(21),
632 8041–8058.
- 633 Uchida, T., Balwada, D., Abernathey, R., McKinley, G., Smith, S., & Levy, M.
634 (2019). The contribution of submesoscale over mesoscale eddy iron transport
635 in the open southern ocean. *Journal of Advances in Modeling Earth Systems*,
636 *11*(12), 3934–3958.
- 637 Uchida, T., Rokem, A., Soler, S., Nicholas, T., Abernathey, R., frederic nouguier,
638 ... Moon, Z. (2023). *xgcm/xrft (v1.0.1)*. [software]. Zenodo. Retrieved from
639 <https://doi.org/10.5281/zenodo.7621857>
- 640 Volkov, D. L., Lee, T., & Fu, L.-L. (2008). Eddy-induced meridional heat transport
641 in the ocean. *Geophysical Research Letters*, *35*(20).
- 642 Waugh, D. W., Banerjee, A., Fyfe, J. C., & Polvani, L. M. (2020). Contrasting
643 recent trends in southern hemisphere westerlies across different ocean basins.
644 *Geophysical Research Letters*, *47*(18), e2020GL088890.
- 645 Wunsch, C. (2020). Is the ocean speeding up? ocean surface energy trends. *Journal*
646 *of Physical Oceanography*, *50*(11), 3205–3217.
- 647 Youngs, M. K., Freilich, M. A., & Lovenduski, N. S. (2023). Air-sea co2 fluxes local-
648 ized by topography in a southern ocean channel. *Geophysical Research Letters*,
649 *50*(18), e2023GL104802.
- 650 Zhang, X., Nikurashin, M., Peña-Molino, B., Rintoul, S. R., & Doddridge, E. (2023).
651 A theory of standing meanders of the antarctic circumpolar current and their
652 response to wind. *Journal of Physical Oceanography*, *53*(1), 235–251.